Theory of subwavelength hole arrays coupled with photonic crystals for extraordinary thermal emission

R. Biswas,[1] C. G. Ding,[1] I. Puscasu,[2] M. Pralle,[2] M. McNeal,[2] J. Daly,[2] A. Greenwald,[2] and E. Johnson[2]
[1]*Department of Physics and Astronomy, Department of Electrical and Computer Engineering, Microelectronics Research Center and Ames Laboratory, Iowa State University, Ames, Iowa 50011, USA*
[2]*Ion Optics Inc., Waltham, Massachusetts 02452, USA*
(Received 11 April 2006; published 11 July 2006)

A subwavelength array of holes in a metal film residing on a silicon photonic crystal exhibits very sharp resonant absorption modes and extraordinary thermal emission. We developed a rigorous electromagnetic theory of subwavelength emitters based on the scattering matrix approach. Simulations exhibit a resonant absorption and emission when the photonic crystal is present, in good agreement with measurements. Diffraction resonances are found within the silicon photonic crystal. These combine with the extraordinary transmission through subwavelength hole arrays to generate resonant absorption in subwavelength arrays of metallodielectric photonic crystals. There is enormous enhancement of fields within the holes for resonant emissive modes.

DOI: 10.1103/PhysRevB.74.045107 PACS number(s): 42.70.Qs, 42.72.Ai, 44.40.+a, 71.36.+c

I. INTRODUCTION

Subwavelength arrays of holes in metal films have recently attracted enormous scientific interest following the discovery of enhanced transmission of light through such periodic arrays.[1] For incident light of wavelength λ, a hole in a metallic sheet cannot sustain propagating modes for hole diameters less than $\sim\lambda/2$. Experimental and theoretical studies have interpreted the enhanced transmission[2,3] to be due to generation of surface plasmons on the metal-dielectric interfaces. Others have argued for multiple diffraction effects.[4,5] Such subwavelength arrays have great potential for novel applications to imaging and optics. Photonic crystals[6] have been extensively studied for wide-ranging applications to light manipulation in optics and optical communications.

I. Puscasu *et al.*[7] and M. Pralle *et al.*[8] recently discovered that subwavelength hole arrays have extraordinary sharp thermal emission that substantially modify the black-body spectrum. By combining a photonic crystal (PC) with the subwavelength hole array in a metal, a narrow resonant absorption was created, leading to a narrow band thermal emission at a wavelength λ near the lattice spacing a. Remarkably, when the subwavelength metal array resides on a uniform substrate, no resonant absorption or emission is observed. We provide a rigorous explanation for these unexpected results using a comprehensive electromagnetic theory of the optical properties. Such subwavelength emitter arrays have immense potential for a new class of infrared sensors of gases and toxic species. If narrow band thermal emission can be tuned to optical wavelengths, remarkable energy efficient incandescent sources can be achieved offering great promise for energy-efficient lighting.

More recently, it has been observed[7] that triangular lattices offer a narrower absorption/emission than the previous square lattices.[8] Previously, the spectral control of thermal emission was achieved by periodic etching of pyramidal pits in a Pt-coated silicon wafer[9] to increase the thermal emission intensity at 2–2.5 μm. Recently, by introducing a periodic one-dimensional microstructure into the polar SiC wafer, a thermal emissive infrared source was fabricated that was remarkably coherent over large distances with radiation in narrow well-defined directions.[10] This is based on the generation of surface phonon polaritons in the polar material.[10]

Infrared emitters: Simulation and measurement

The emissive structure developed by I. Puscasu *et al.*,[7] utilized n-silicon wafers coated with a thin Pt layer (thickness $d_1 \sim 0.1$ μm; see Fig. 1). A triangular lattice of holes was fabricated by standard photolithography and deep reactive ion-beam etching. The lattice spacing (a), hole radius (r), and etching depth d_3 were varied systematically. At small etch depths ($d_3 \sim 0.1$ μm), holes are in the metal. For deeper etches in the silicon, there is a hole array in the metal mesh residing on a two-dimensional (2D) silicon photonic crystal

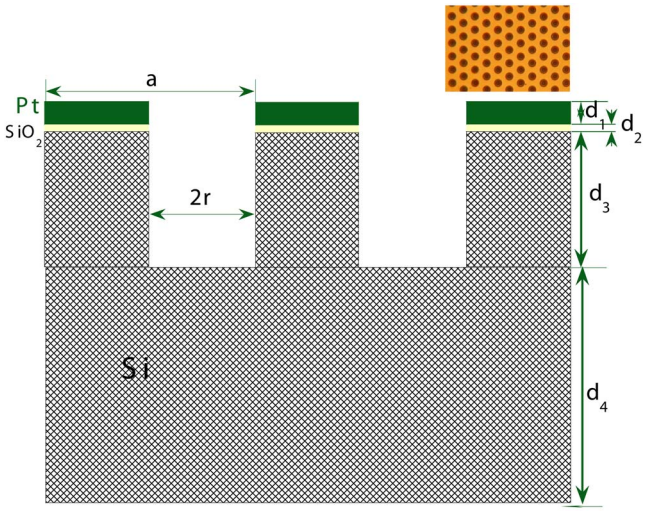

FIG. 1. (Color online) Schematic of subwavelength structure in side view, showing metal coating, silicon photonic crystal and substrate, with the thicknesses of the layers displayed. The top view of the experimental structure is shown in the top right.

with the same triangular symmetry. We focus on the $a=4.2$ μm lattice since measurements on $a=3.4-6.2$ μm produced similar results. For $r=0.25a=1.05$ μm, a subwavelength hole array was formed for $\lambda>4$ μm.

The reflection (R) and transmission (T) of these structures were measured with high resolution Fourier transform infrared spectroscopy (FTIR).[7] The absorption $A=1-R-T$. The measured transmission (T) is close to 0, and the calculated transmission in this paper is less than 0.006. Hence $T \ll 1$ and $A \cong 1-\mathrm{R}$. An absorption peak is then equivalent to a reflectance minimum. If the substrate was thinned away to zero, the reflection minima would correspond to a transmission peak as in the subwavelength arrays.[1–3]

To understand the unexpected emission, we developed a rigorous scattering matrix (S-matrix) theory.[11] The structure is divided into slices along z. In each slice, the dielectric function $\epsilon(\mathbf{r})$ is a periodic function of the planar coordinates (x,y). Hence, the dielectric function and its inverse is expressed as a Fourier expansion with coefficients $\varepsilon(\mathrm{G})$ or $\varepsilon^{-1}(\mathrm{G})$. In the triangular lattice, the lattice vectors are $\mathbf{A}_1=a(1,0)$, $\mathbf{A}_2=a(1/2,\sqrt{3}/2)$ with reciprocal lattice vectors $\mathbf{G}_1=(2\pi/a)(1,-1/\sqrt{3})$, $\mathbf{G}_2=(2\pi/a)(0,2/\sqrt{3})$.

In the metal layer

$$\varepsilon(G)=\{\varepsilon(\omega)+f[1-\varepsilon(\omega)]\}\delta_{G,0}+f[1-\varepsilon(\omega)]\frac{2J_1(Gr)}{Gr}.$$

The air filling fraction $f=\pi r^2/(\sqrt{3}a^2/2)$ and ω is the frequency. The E and H fields are expanded in Bloch waves,

$$E_k(x_\parallel,z)=\sum_G E_G(z)e^{i(k+G)\cdot x_\parallel}.$$

The transfer matrix[11] is diagonalized to obtain the eigenmodes of both polarizations within each layer. Continuity of the parallel components of **E** and **H** at each interface, lead to the scattering matrices S_i of each layer. A standard recursion algorithm[12] combines the scattering matrices of each layer into the scattering matrix S for the entire structure, from which we simulate the reflection and transmission.

We utilize the Drude form $\varepsilon(\omega)$ of Pt incorporating absorption, fitted to the experimentally measured $\varepsilon(\omega)$.[13] We obtained very similar results with the interpolated experimental ω-dependent $\varepsilon(\omega)$ for Pt. For Si, we utilize $\varepsilon=\varepsilon_1+i\varepsilon_2$, with $\varepsilon_1=11.7$ a value reasonable throughout IR wavelengths. By fitting measured reflection and transmission through silicon wafers without metal coatings,[14] we found a weak absorption $\varepsilon_2=0.02$ was needed to account for measurements.

In the metal, $\varepsilon(\mathrm{G})$ has significant Fourier components for large holes ($r/a=0.25$) and strongly damped components for smaller holes. Convergence for most frequencies were obtained by $N(G)=535$ plane waves $[|G|<14(2\pi/a)]$ for $r/a=0.25$, and matrix sizes $[2N(G)]$ of 1070. Higher convergence was achieved at selected frequencies using $N(G)=757$. Larger holes with $r/a=0.35$, necessitate using $N(G)=757$ for a large portion of the frequency range. For smaller holes (e.g., $r/a<0.25$) or for all-dielectric structures convergence is faster, and was achieved with $N(G)\sim 271$.

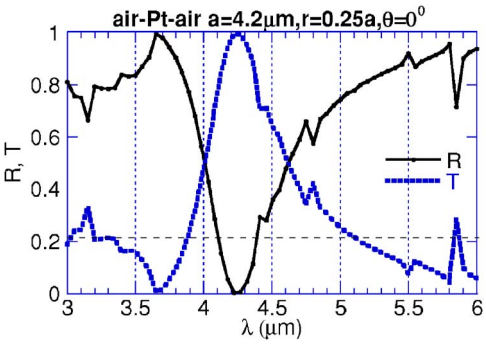

FIG. 2. (Color online) Calculated reflectance (R) and transmission (T) of a subwavelength triangular lattice of holes of radius $r/a=0.25$ in a thin Pt layer of thickness 0.1 μm at normal incidence.

II. RESULTS

To understand the complex multilayer metallodielectric PC, we conceptually divide it into simpler components. We then understand the optical properties of the composite structure. We first simulated a freestanding metal mesh and find (Fig. 2) a deep resonance near $\lambda \sim a$, where the transmission $T \sim 1$, the reflectance $R \sim 0$ in agreement with the enhanced transmission in subwavelength hole arrays. The transmission is more than four times the predicted classical transmission (0.22) for air holes with this area. For smaller holes, the T peak remains at $\lambda \sim a$, but becomes narrower and weaker, and the enhancement factor increases further. The hole array selectively filters a narrow band of wavelengths around $\lambda \sim a$ to pass with enhanced transmission. The enhanced transmission in the triangular lattice is similar to previous results with square lattices.[1–5,14] We have examined in detail the origin of the enhanced transmission mode,[15] and find that the enhanced transmission in freestanding metal mesh is due to a diffraction of the incident wave. Constructive interference between the reflected evanescent surface waves and the incident field occurs at the resonant frequency of the transmission maximum. The calculation will be described separately.[15]

We now analyze the full structure with the thin (0.1 μm) Pt coating covering the photonic crystal (depth d_3) on a thick ($d_4=372$ μm) Si wafer. A thin oxide (thickness 0.1 μm) separates the metal and silicon. The calculated normal reflectance (Fig. 3) shows a deep minimum at $\lambda \sim 4$ μm with a weaker longer λ minima at 10.7 μm. The transmission through the thick wafer is below 0.006 at all wavelengths and is not shown. The main resonance contains a sharp subminima near 4.25 μm ($\lambda \sim a$). The wavelengths of the Pt-semiconductor surface plasmon (SP) (Ref. 16) (Fig. 3) are shown for the effective dielectric ($\varepsilon_{\mathrm{eff}}=9.27$) appropriate for the air filling fraction (23%) of the Si PC. The dip near 11 μm varies as $\sqrt{\epsilon_{\mathrm{eff}}}$ for different filling ratios and can be identified with the $(i=1,j=0)$ Si-Pt SP. The (3,0) Si-Pt SP occurs within the main minima. The main resonance is controlled by the metal-air enhanced transmission mode. For $\lambda < a$, the specular R has lower values ($R=0.5-0.6$) than nonspecular R (Fig. 3) due to diffraction.

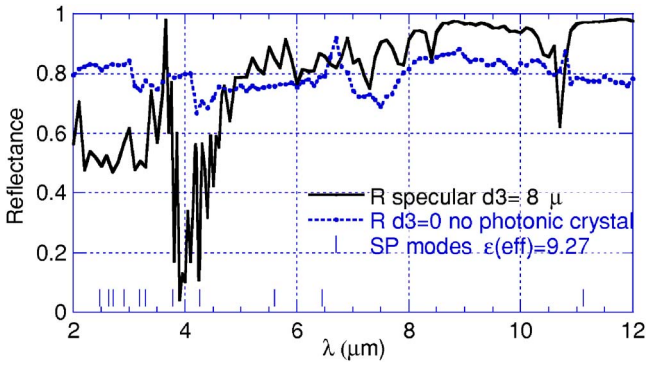

FIG. 3. (Color online) Calculated specular reflectance (R) at normal incidence photonic crystal of $d_3=8$ μm on the subwavelength metal mesh of thickness $d_1=0.1$ μm. The entire structure resides on a thick (372 μm) Si wafer. Also shown (bars) are the positions of the surface plasmon modes for a metal-dielectric interface with effective dielectric constant of 9.27 of the patterned Si-layer. The dotted line shows the reflectance when there is no photonic crystal ($d_3=0$), i.e., a uniform silicon substrate. The transmission through the silicon wafer is below 0.006 at all wavelengths and is not shown in the graph.

Remarkably, when the subwavelength hole mesh in the metal layer resides on a uniform Si-substrate, the reflectance (Fig. 3) exhibits only a weak dip near $\lambda \sim a$. From calculations, we verified that PC depths exceeding ~ 4 μm give similar results as $d_3=8$ μm. The depth effect on the resonance saturates after 4 μm.

Similar calculated spectral features (Fig. 4) occur for off-normal incidence ($\theta=10°$) where the main resonance red-shifts to 4.5 μm (for p polarization). The reflectance oscillations occur due to multiple reflections within the layered structure. The measured reflectance for this structure for $\theta=10°$ (Fig. 4) was obtained with an FTIR spectrometer. Calculations agree well with measurements, except for a shift, including the deep minimum ($R \sim 0.1$) at $\lambda \sim a$, the long λ minimum near 10.5 μm the high R at long λ and the lower R for $\lambda < a$. The calculated absorption $A=1-R-T$, has a principal peak at $\lambda \sim a$. The calculated emission is the black-

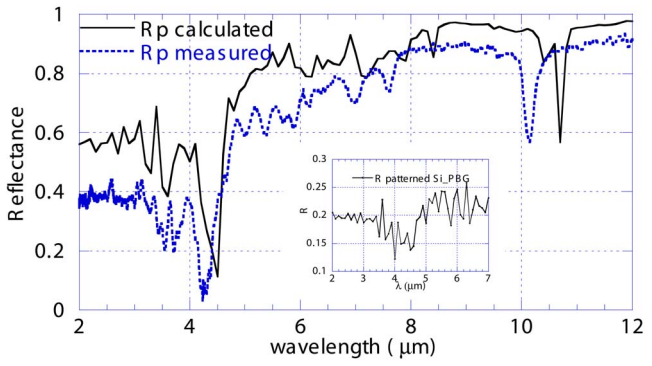

FIG. 4. (Color online) Calculated off normal specular reflectance ($\theta=10°$, $\phi=0°$) in p polarization for the $d_3=8$ μm structure, compared to measured p-polarized specular reflectance (dotted line). The calculated reflectance from a patterned silicon wafer (without the metal coating) and with $a=4.2$ μm is shown in the inset.

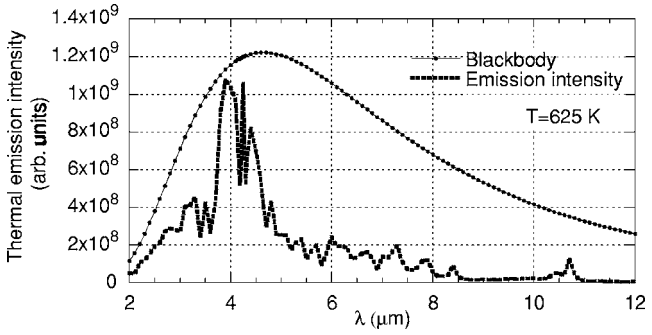

FIG. 5. Calculated emission in the normal direction at $T=625$ K for the structure with a photonic crystal of depth $d_3=8$ μ on a subwavelength metal mesh, compared with the expected black-body curve (dotted line).

body Planck function modulated by the absorption. At temperatures typical of experiment (625 K), we calculate a normal emissivity (Fig. 5), centered at a wavelength λ just less than a, with magnitude just below the black-body emission. The theoretical emission spectrum agrees well with measurement.

Dependence on the hole radius

We have systematically studied the dependence of the optical properties on the hole radius and found considerable insight into the underlying mechanisms. It is well known that cylindrical apertures allow a propagating $TE11$ mode below a cutoff wavelength $\lambda_{11}=3.42r$ (~ 3.6 μm for our geometry with $r=0.25a$), below which the holes partially transmit as seen in Fig. 3. It is essential that the holes be of subwavelength dimension with the condition that the cutoff wavelength for propagating modes be smaller than the lattice spacing (a). If the hole radius increases, the wavelength cutoff λ_{11} increases, and the apertures are subwavelength when $\lambda_{11} < a$ or $r/a < 0.29$ (for cylindrical apertures). When $r/a > 0.29$ additional wave-guide modes transmit through the apertures leading to a much broader reflection minimum, and the structure is no longer in the subwavelength regime. Alternatively, for smaller hole radius the wavelength cutoff λ_{11} becomes shorter. To understand further the mechanism of enhanced absorption, we have simulated the optical behavior for structures with holes of different sizes. For small holes ($r/a=0.20$), the reflectance minimum at $\lambda \sim a$ is present but weaker in magnitude with $R \sim 0.4$ at the minimum. This leads to a narrow but weaker intensity absorption peak, so that the emission from this structure is considerably lower than the black-body value. Decreasing hole radii leads to narrower but shallower reflection minima. For still smaller r/a, the reflectance minimum decreases in size further, and the reflectance approaches a high featureless value as expected for the limiting case of a smooth metal film. For $r/a=0.25$, the reflectance minimum is narrow and R is ~ 0.1 at the minimum leading to a deep absorption that translates into a narrow and strong emission peak. The wavelength of the absorption minimum does not appreciably change with hole radius for these small holes ($r/a \leq 0.25$), since the resonance is controlled by the porous metal mesh.

As the holes are made larger $r/a=0.30$, the reflectance minimum broadens significantly and there is considerable absorption in the range of 5–7 μm. The reflectance is dominated by multiple reflectance oscillations throughout this wavelength range. For still larger radius ($r/a=0.35$), the entire reflectance feature broadens into a single feature with considerable multiple reflectance oscillations. The transmitted waveguide mode is now at 5 μm, indicative of the dip near 5 μm (Fig. 6, $r/a=0.30$). We find the value of $r/a=0.25$ to be very close to the optimum radius that ensures both high absorbance and emittance as well as a narrow absorption profile.

The long wavelength reflectance minimum varies from 10.7 μm ($r/a=0.25$) to 9.2 μm ($r/a=0.35$). The wavelength of this feature scales linearly with the effective refractive index (n_{eff}) of the silicon photonic crystal. This behavior is consistent with this feature arising from the metal-semiconductor surface plasmon mode at the silicon-metal interface.

To understand the role of the PC we calculated the reflectance of the 2D PC without the metal overlayer, for propagation along z for different values of the hole radius r/a. In the limit of vanishing hole radius, the reflectance approaches the featureless value of ~0.3 expected for a smooth dielectric film. For small hole radius ($r/a=0.15-0.20$), the reflectance is featureless (Fig. 7) with typical values of $R \sim 0.2-0.25$. For larger holes with $r/a>0.25$, we find weak but significant reflectance dips near $\lambda \sim a$ where $R \sim 0.15$, lower than typical reflectance values of 0.2–0.25 in the 2–7 μm range. The fitted curves (Fig. 7) illustrate weak but significant reflection minimum for $r/a>0.25$. For larger holes ($r/a=0.3-0.35$), there is an overall decrease of the reflectance around $\lambda \sim a$, accompanied by strong oscillations from multiple reflection effects. The silicon photonic crystal behaves similar to a two-layer material with a smaller effective refractive index (n_{eff}) in the upper layer of thickness 8 μm, on top of the much thicker silicon substrate ($n=3.42$). The 8 μm thickness and n_{eff} control the multiple reflection oscillations.

III. DISCUSSION

At the resonances, for p-polarized incident waves, calculated E field intensities for the full structure at the top surface [Fig. 8(a)] show sharp maxima at the rim of the holes with large enhancements exceeding the incident field at these maxima. Fields are weaker near the center of the hole. For the $\lambda=4.25$ μm subpeak, the field is dipolar, consistent with a diffraction mode in the subwavelength hole array in the metal. The reasoning here is that we examined the fields of the enhanced transmission mode (Fig. 3) of the hole array in the metal layer and found a very similar field distribution as in Fig. 8(a). The high fields at the hole edges extend from the top surface to the bottom of the metal layer. The diffractive contributions to the fields of the enhanced transmission case are discussed below.

We consider the $r/a=0.25$ case in particular, in which the silicon PC exhibits a weak reflectance minimum at $\lambda \sim a$ (Fig. 7). The PC diffracts[5] a guided mode along z (perpendicular to the layer), with the modal field in the silicon PC having maxima at the edges of the holes along x (the direction of a crystal lattice vector), and appreciable in the Si regions away from the holes [Fig. 8(b)]. The symmetry of the

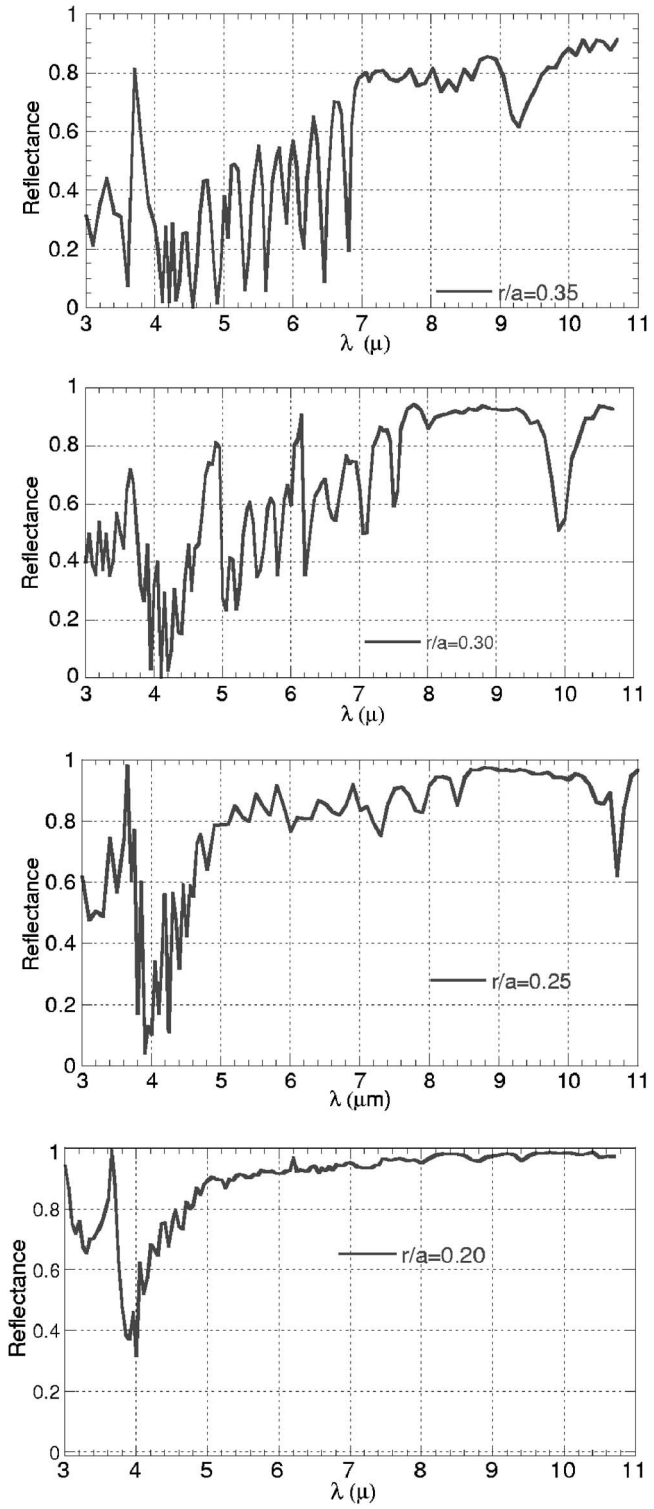

FIG. 6. Calculated normal reflectance of the subwavelength hole array in a metal layer, on the photonic crystal (Fig. 1) as a function of hole size with r/a varying from 0.20 to 0.35. All other parameters in the structure are kept the same as the photonic crystal case in Fig. 3 (including the depth $d_3=8$ μm and $d_4=372$ μm).

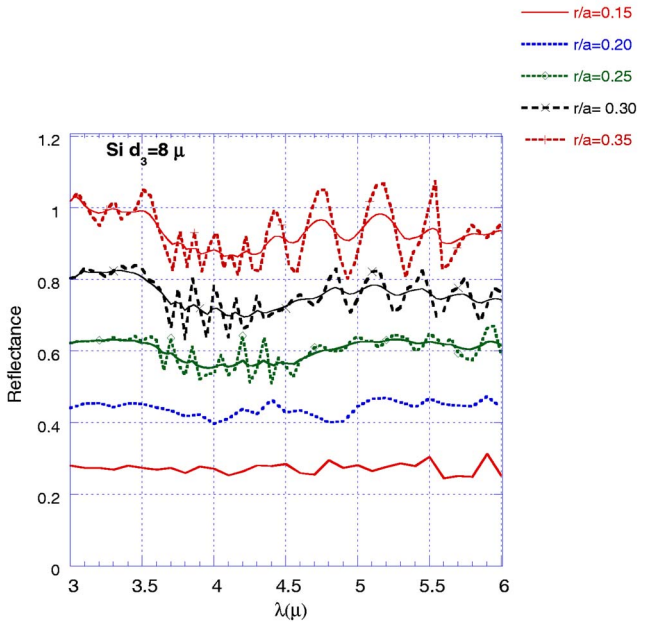

FIG. 7. (Color online) The calculated reflectance from a patterned silicon wafer (without the metal coating) with $a=4.2$ μm and for different values of the hole radius $r/a=0.15$ to 0.35. For clarity, each curve is offset upward by 0.2. Solid lines in the top three curves are fits.

field is due to the incident wave being polarized along the x axis, and this mode is sixfold rotationally degenerate. There is no guided mode for a uniform substrate.

The diffraction resonance in the silicon PC for $r/a=0.25$ has a field distribution of similar symmetry as in the metal layer, and matches well with the extraordinary transmission resonance of the subwavelength hole array in the metal. These two resonances couple to guide the incoming mode into the PC. Since the PC weakly absorbs, this mode is absorbed within the Si-PC and the substrate. Thermal emission is the reverse process where the spontaneous emission of photons within Si emerges from the surface of the metal mesh at the resonance $\lambda \sim a$. This mechanism differs from directive thermal emission from three-dimensional (3D) metallic PCs.[17–20]

The radius of $r/a=0.25$ allows the guided mode to diffract through the silicon PC. Although larger holes also allow a guided mode in the PC (Fig. 6), the porous metallic grid now supports propagating wave-guide modes for holes that are larger than $r/a=0.29$. There is considerable transmission through the porous metallic layer for $r/a>0.29$, and a broad reflection feature and consequently broad absorption feature emerges. The emission from such a structure is no longer a narrow band, as is the case for the subwavelength lattice with $r/a=0.25$. Hence, the value of $r/a=0.25$ is close to the optimum geometry for a enhanced transmission mode through a subwavelength array that can be coupled to a guided mode in the underlying silicon PC. These numerical results provide insight into the modes expected in this structure and account for most of the numerical and experimental results. More rigorous treatments of thermal radiation coupled to photonic crystal modes[19,21] have recently been developed.

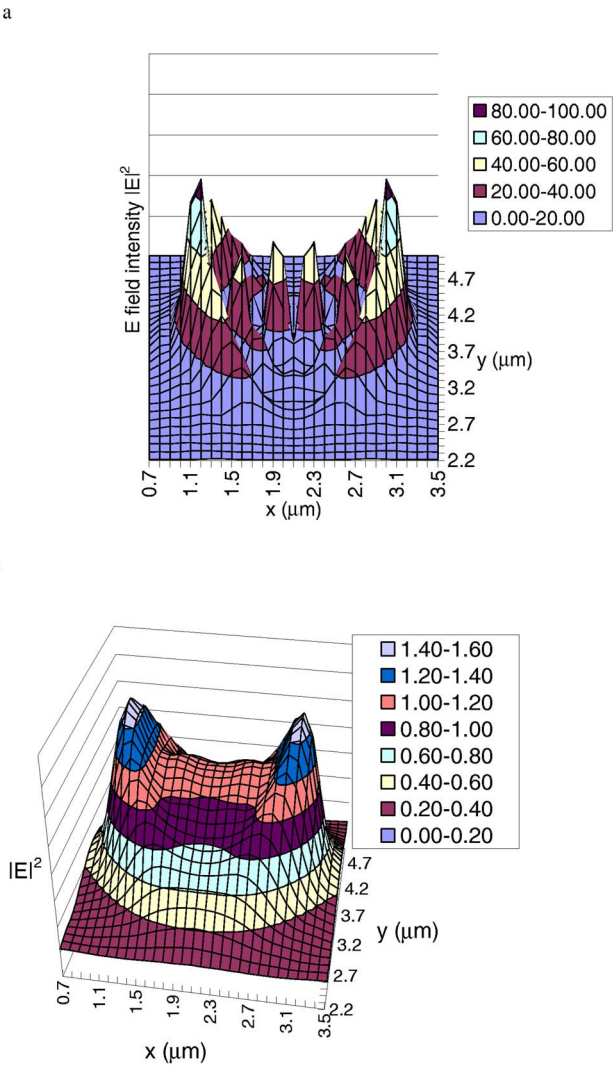

FIG. 8. (Color online) (a) Electric field intensities plotted at the surface of the metal layer, at the resonant wavelengths of 4.25 μm, showing large field enhancement at the hole boundaries. (b) **E** field intensity just below the surface for the resonant mode through the silicon PC without the metal layer at $\lambda \sim 4.46$ μm.

The low order $k=0$ photonic bands occur at $\lambda \sim n_{\text{eff}} a \sim 3a$, or at wavelengths much longer than the resonant emission region, and are therefore not connected with the observed emission. We have briefly considered different ϵ substrates. We find that small decreases in ϵ leave the resonant absorption mode near $\lambda \sim a$, while the long wavelength reflectance minimum (10.7 μm for Si substrates and $r/a=0.25$ in Fig. 3) moves to lower wavelengths scaling as n_{eff} similar to the effect found for larger holes (Fig. 6). This supports the conclusion that this long wavelength mode is a metal-semiconductor surface plasmon mode. As ϵ is weakened, the guiding of modes within the substrate also decreases. In the limit of $\varepsilon \to 1$, the guiding mode vanishes as it must. However, the limit $\varepsilon \to 1$ is the limit of a thin metal mesh surrounded by air—exactly the result of Fig. 2. This $\varepsilon \to 1$ limit produces a deep reflectance minima and strong transmission maxima (as in Fig. 2). However, there is no

absorbance in the $\varepsilon \rightarrow 1$ limit. This is why small decreases in ϵ do not change much the reflectance dip near $\lambda \sim a$, although the absorption is weaker since transmission through the metal mesh also increases. Further experimental and simulation studies are needed to quantify the semiconductor substrates. It should be noted that the metal-dielectric SPs change position with changing ϵ, so that individual emission peaklets occur at different λ, affording an alternate way to tailor the fine features of the emission spectrum.

The resonant emission at $\lambda \sim a$ is controlled instead by the metal mesh. By analyzing the evanescent fields, we inferred that the enhanced transmission is caused by the constructive interference of evanescent diffracted reflected waves with the incident field at the top surface of the metal mesh. These evanescent reflected fields do not contribute to the reflectance of the structure, since reflectance arises from propagating modes. For the wavelength λ just larger than a, the diffracted evanescent waves constructively couple with the incident field, causing the extraordinary transmission through the holes. At wavelengths away from the resonance, the constructive interference effect no longer occurs. The phase of the diffracted wave is controlled by the spacing between holes and not the hole radius. This is why the wavelength of the resonance is controlled by the hole spacing and not affected much by the hole radius. More numerical results will be presented separately[15] to quantify these conclusions. This constructive interference effect controlling the enhanced transmission is independent of the underlying substrate, but must couple to guided modes in the photonic crystal underneath.

IV. CONCLUSIONS

We developed a rigorous scattering-matrix theory of light guidance and emission that can be achieved by coupling a subwavelength array with a photonic crystal, with resonant reflectance minima and emission peaks. The enhanced transmission mode of the subwavelength array of holes in a metal film is guided and absorbed in a photonic crystal with weak absorption. The photonic crystal below the subwavelength metal grid is essential for a strong resonance and high emissivity. Emissive modes have field enhancements at the hole perimeters. Such subwavelength grids have extensive applications for spectroscopic sensors and photon recycling for thermophotonics.

ACKNOWLEDGMENTS

We thank S. Neginhal for computational assistance. This work was partially supported by the National Science Foundation through Grants No. DMR-0346508, No. DMI-0450397, and No. ECS-0601377. The Ames Laboratory is operated by Iowa State University for the U.S. Department of Energy under Contract No. W-7405-Eng-82.

[1] T. W. Ebbesen, H. J. Lezec, H. F. Ghaemi, T. Thio, and P. A. Wolff, Nature **391**, 667 (1998).
[2] L. Martin-Moreno, F. J. Garcia-Vidal, H. J. Lezec, K. M. Pellerin, T. Thio, J. B. Pendry, and T. W. Ebbesen, Phys. Rev. Lett. **86**, 1114 (2001).
[3] L. Martin-Moreno, F. J. Garcia-Vidal, H. J. Lezec, A. Degiron, and T. W. Ebbesen, Phys. Rev. Lett. **90**, 167401 (2003).
[4] M. M. J. Treacy, Phys. Rev. B **66**, 195105 (2002).
[5] H. Lezec and T. Thio, Opt. Express **12**, 3629 (2004).
[6] J. D. Joannopoulos, R. D. Meade, and J. N. Winn, *Photonic Crystals* (Princeton University Press, Princeton, NJ, 1995).
[7] I. Puscasu, M. Pralle, M. McNeal, J. Daly, A. Greenwald, E. Johnson, R. Biswas, and C. G. Ding, J. Appl. Phys. **98**, 013531 (2005).
[8] M. U. Pralle, N. Moelders, M. P. McNeal, I. Puscasu, A. C. Greenwald, J. T. Daly, E. A. Johnson, T. George, D. S. Choi, I. El-Kady, and R. Biswas, Appl. Phys. Lett. **81**, 4685 (2002).
[9] H. Sai, H. Yugami, Y. Akiyama, Y. Yanamori, and K. Hane, J. Opt. Soc. Am. A **18**, 1471 (2001).
[10] J-J. Greffet, R. Carminati, K. Joulain, J-P. Mullet, S. Mainguy, and Y. Chen, Nature **416**, 61 (2002).
[11] Z. Y. Li and L. L. Lin, Phys. Rev. E **67**, 046607 (2003).
[12] L. Li, J. Opt. Soc. Am. A **13**, 1024 (1996).
[13] *Handbook of the Optical Constants of Solids II*, edited by E. Palik (Academic Press, Boston, 1991).
[14] K. L. van der Molen, K. J. Klein Koerkamp, S. Enoch, F. B. Segerink, N. F. van Hulst, and L. Kuipers, Phys. Rev. B **72**, 045421 (2005).
[15] R. Biswas *et al.* (unpublished).
[16] H. Raether, *Surface Plasmons* (Springer-Verlag, Berlin, 1988).
[17] S. Y. Lin, J. Moreno, and J. G. Fleming, Appl. Phys. Lett. **83**, 380 (2003).
[18] C. H. Seager, M. B. Sinclair, and J. G. Fleming, Appl. Phys. Lett. **86**, 244105 (2005).
[19] I. El-Kady, W. W. Chow, and J. G. Fleming, Phys. Rev. B **72**, 195110 (2005).
[20] S. Enoch, J.-J. Simon, L. Escoubas, Z. Elalmy, F. Lemarquis, P. Torchio, and G. Albrand, Appl. Phys. Lett. **86**, 261101 (2005).
[21] C. Luo, A. Narayanaswamy, G. Chen, and J. D. Joannopoulos, Phys. Rev. Lett. **93**, 213905 (2004).